Modeling Studies of Photoionization Experiments Driven by Z-pinch X-rays

Nathan C. Shupe

nshupe1@swarthmore.edu

1. Introduction

1.1. What type of astrophysical objects?

Photoionized plasmas are characteristic of some of the brightest x-ray sources in the sky, including but not limited to black hole and neutron star binaries (x-ray binaries) and active galactic nuclei (quasars). In a high mass x-ray binary system (HMXRB), the compact object (a black hole or neutron star) can capture some of the material released in the stellar wind of a nearby giant star. An artist's conception of such a system in shown in Fig. 1. As the material spirals toward the compact object, its gravitational energy is converted to thermal kinetic energy. Hard (high-energy) x-rays generated in the accretion disk photoionize the nearby cool circumstellar gas and produce radiation in the form of radiative recombination continua and recombination cascades (3).

In 1999, the launch of the National Aeronautics and Space Administration's Chandra and the European Space Agency's XMM-Newton x-ray telescopes made available to the scientific community for the first time new high-resolution spectroscopy of astrophysical phenomena. The advent of these telescopes and their accompanying high resolution spectroscopy has fueled the demand for a high degree of accuracy in our spectral models. Much work already has been done in developing spectral models for coronal plasmas, while significantly less work has been devoted to the development of spectral models for photoionized plasmas (2). The apparent lack of well tested spectral models for photoionized plasmas means that at present we cannot be certain of the accuracy of our interpretation of the spectra from these sources. Therefore, until we benchmark and test our spectral models for photoionized plasmas, many of the brightest cosmic x-ray sources will continue to be unavailable for detailed and accurate spectroscopic investigations.

1.2. Differences between photoionized spectrum and coronal spectrum

The two main classes of x-ray sources differ mostly in the process that dominates excitation, de-excitation, and ionization for each. A collisionally dominated (or coronal) plasma is

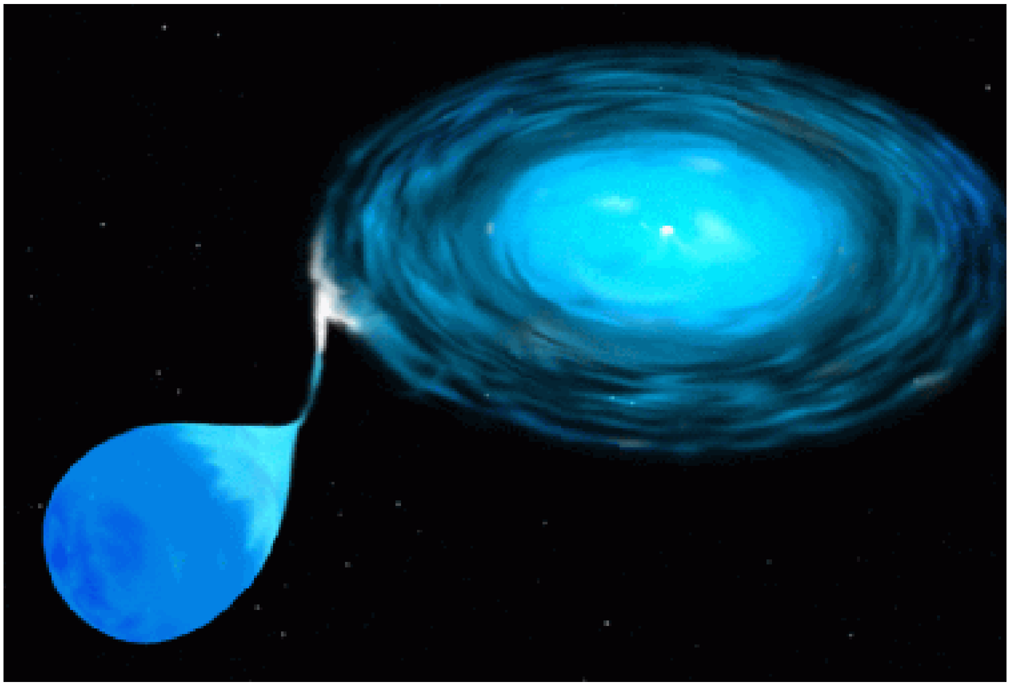

Fig. 1.— An artist conception of an x-ray binary. Pictured is a compact object gravitationally capturing wind material from a nearby blue giant star. This captured wind material spirals toward the compact object and forms an accretion disk. The inner parts of this accretion disk are extremely hot and emit radiation in the x-ray band of the electromagnetic spectrum.

so named because collisions are the driving force of heating in the plasma. Electron impacts with ions populate excited levels and electron-ion collisions are the main source of ionization. The equation of ionization equilibrium for a collisionally dominated plasma can be written as equivalence between the ionization processes and the recombination processes:

$$n_e C_i n_i = n_e \alpha_{i+1} n_{i+1}, \tag{1.1}$$

where n_e (cm^{-3}) is the electron number density, n_i is the number density of ions of charge state i, n_{i+1} is the number density of ions of charge state $i+1$, C_i (cm^3 s^{-1}) is the collisional ionization rate for ions with charge state i, and α_{i+1} (cm^3 s^{-1}) is the recombination rate (for both dielectric and radiative recombination) for ions with charge state $i+1$. Solving for the ionization balance, $\frac{n_{i+1}}{n_i}$, we find that it is completely determined by the ratio of the *temperature* dependent rates C_i and α_{i+1}. Thus, the temperature sets the ionization balance in a coronal plasma, and for an x-ray emitting plasma is of order several hundred eV.

The temperature, however, is not the only dependent variable in setting the ionization balance of a photoionized plasma. Rather, we find that there is a new term on the left side of

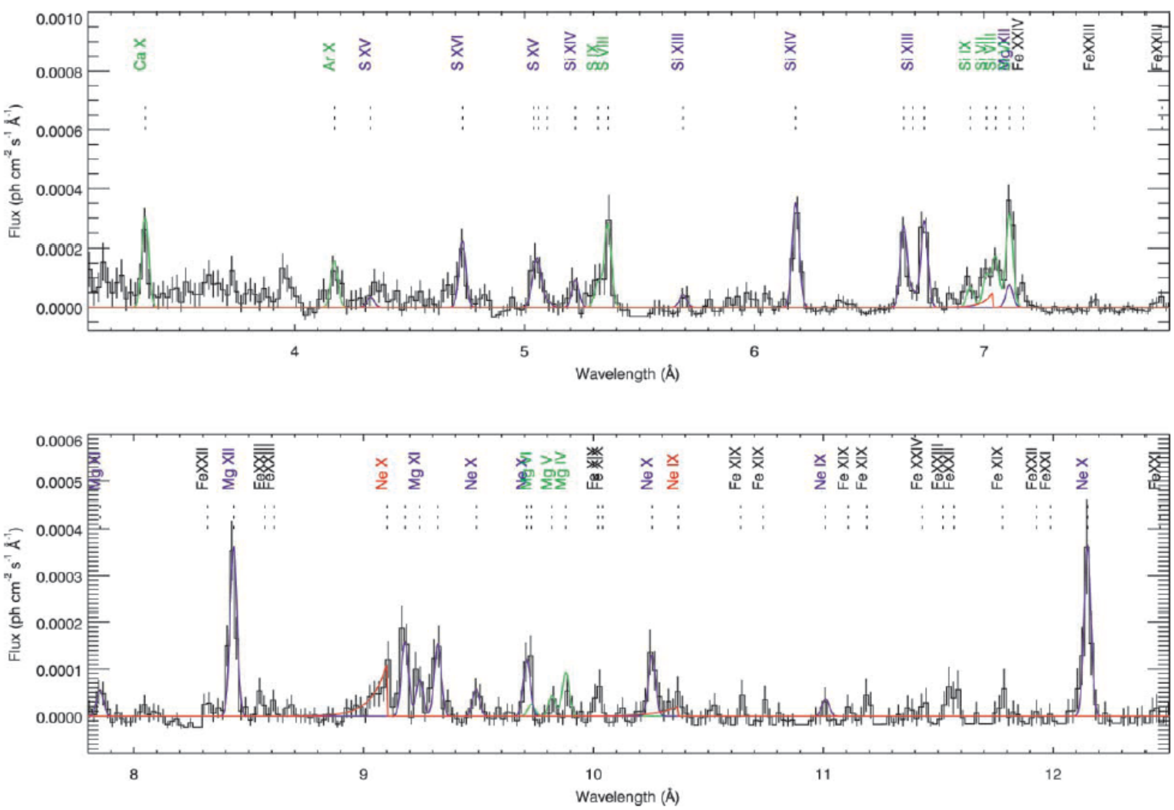

Fig. 2.— A high-resolution X-ray spectrum of the ionized stellar wind of Vela X-1 during eclipse captured with the High-Energy Transmission Grating Spectrometer (HETGS) on board the Chandra X-ray Observatory. The fluorescent lines are plotted in green, the highly ionized lines in blue, and the radiative recombination continua (which are characteristic of a photoionized plasma) in red. (6)

the ionization equilibrium equation which takes into account the photoionization processes. Thus, in these plasmas, ionization is driven both by electron temperature and by an ionizing flux of radiation. As a result, in a photoionized plasma it is possible to achieve the same degree of ionization as a coronal plasma with a lower electron temperature. The degree to which the plasma is *overionized* relative to its electron temperature is fully determined by the ionization parameter, ξ, which we will define and derive in a later section.

As one might expect, the spectra obtained from these two classes of plasma have distinct differing features. Since x-ray coronal plasmas are at higher temperatures, ionization is primarily balanced by dielectronic recombination (excess energy of the recombined electron is used to excite another ionic electron, making the ion doubly-excited), while the cooler photoionized plasmas balance ionization with radiative recombination (excess energy of the recombined electron is radiated away) and cascade following recombination (3).

Shown in Fig. 3 and Fig. 4 are model emission rate spectra for a coronal and a photoionized plasma respectively. Notice that certain line features of the coronal spectrum are not present in the photoionized spectrum. Since the processes governing electronic transitions and ionization differ between the two classes, any spectral model of an x-ray source should employ an atomic model specific to the class of that source. That is, even if we have well-developed atomic models for one class of x-ray source (as we do for coronal plasmas), we cannot apply these models to interpret spectra from sources of the other class (in this case, photoionized plasmas). Thus, accurate interpretation of x-ray spectra requires that we have accurate spectral models for each class of sources.

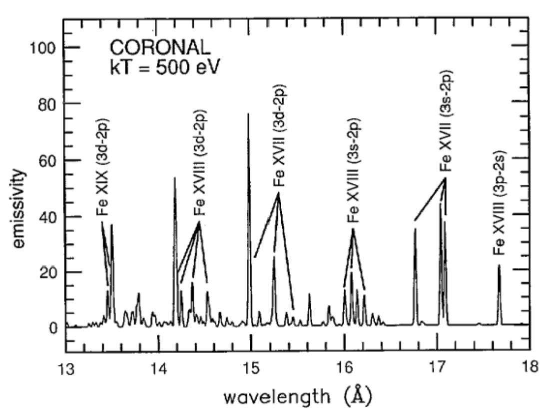

Fig. 3.— Iron Model Emission Rate Spectrum for a Coronal Plasma, $kT_e = 500$ eV, $n_e = 10^{11}$ cm^{-3}.

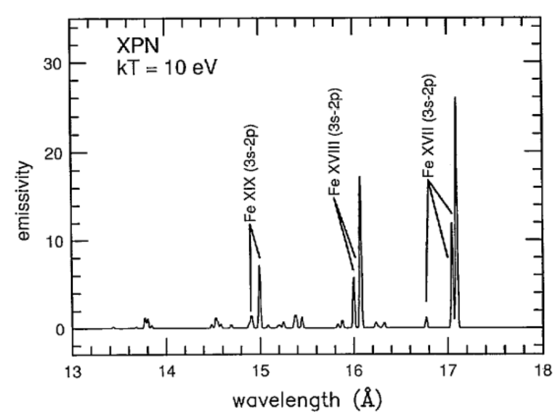

Fig. 4.— Iron Model Emission Rate Spectrum for a Photoionized Plasma, $kT_e = 10$ eV, $n_e = 10^{11}$ cm^{-3}.

1.3. What's the point of doing experiments in the lab?

Traditionally, astrophysics has not been included in the category of laboratory sciences. That is, since the scales and environments in which astrophysical phenomena occur differ so dramatically from anything we have been able to reproduce in the laboratory, the study of these phenomena has been limited to observation and computer modeling. That is not to say that observation and computer modeling are not effective procedures, for certainly the opposite is true, but there does exist a problem inherent to these procedures in that the only calibration of the model is the data the model is trying to explain. Essentially this means that models calibrated only by observational data tend to preferentially fit the data from some sources better than from other sources, unless certain parameters in the model are adjustable. Ideally, we would like to have models that have no adjustable or free parameters, which would indicate that we have sufficiently modeled the physics governing the situation in order to constrain the values for the parameters.

Like observations of cosmic sources, laboratory experiments provide a source of data by which spectral codes can be tested and benchmarked. Unlike observations, however, laboratory experiments provide an environment in which the emitting plasma can be controlled and characterized. That is, in laboratory experiments, we can control what type of gas is irradiated, the position of the gas relative to the x-ray source, and the magnitude of x-rays which irradiate the gas, while also being able to directly observe the plasma and characterize some of its properties. Therefore, the local and more versatile laboratory experiments allow us to more readily benchmark the atomic kinetics models used to interpret the spectra from photoionized plasmas.

1.4. Brief description of gas cell experiments

A series of ride-along gas cell shots have been conducted at the Sandia National Laboratories Z pulsed power accelerator (see 1.6 for a description of the facility). The experimental package consists of a cm-scale neon filled cell with mylar windows, mounted several cm from the anode current return can, inside of which lies the Z-pinch. In this configuration, the pinch is analogous to the x-ray emmitting accretion disk in an x-ray binary, and the gas in the cell is like the photoionized circumstellar gas. Experiments already completed have used neon of density $n_{ion} \sim 10^{18}$ cm^{-3} observed in absorption (the pinch serves as the backlighter) with a time-integrated spectrometer. For future experiments, we plan to make simultaneous time-resolved emission and absorption spectroscopic measurements along the lines of sight pictured in Fig. 5.

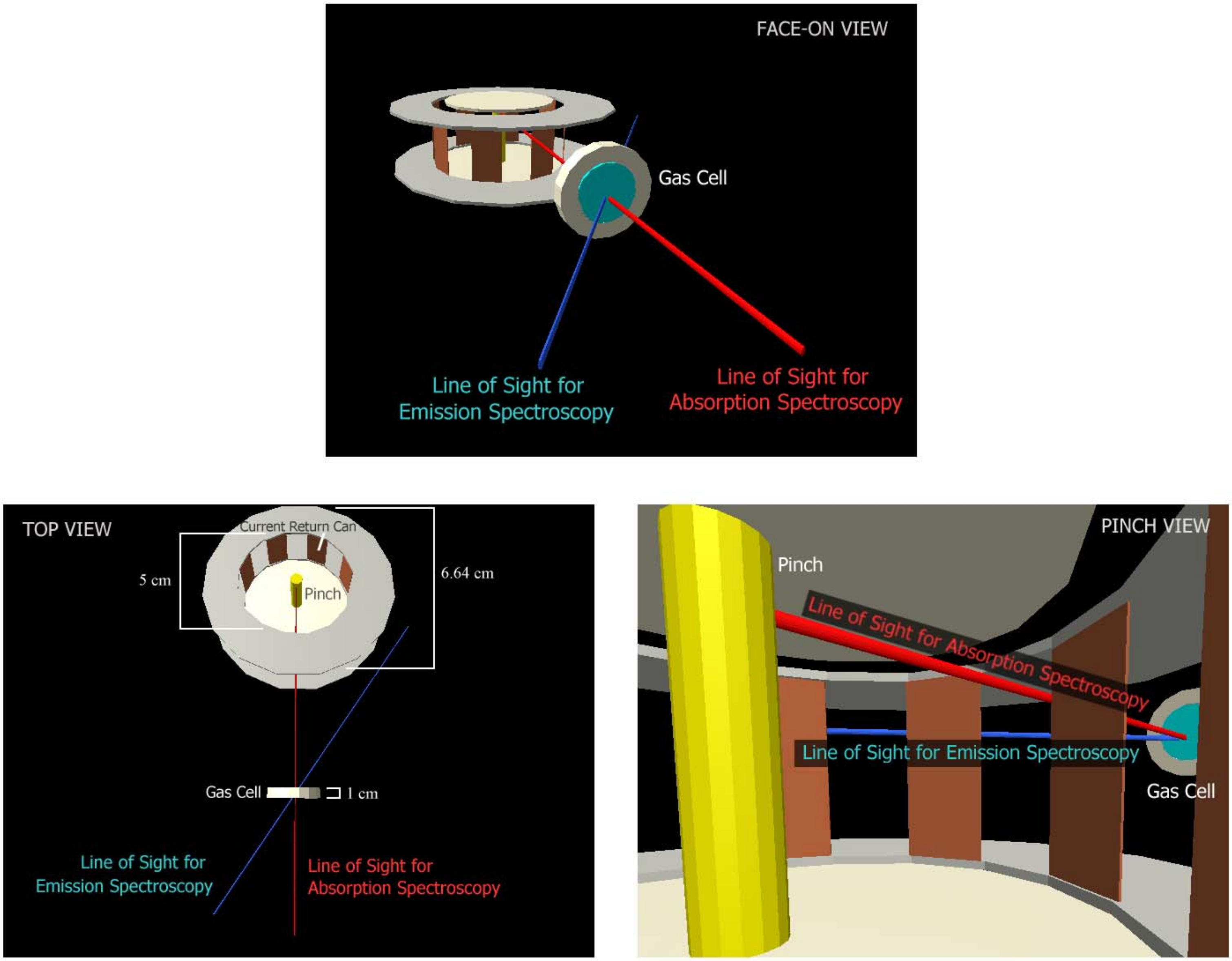

Fig. 5.— Face-on, top and pinch views of the experimental set up, with the spectroscopic lines of sight shown in red and blue. Note that the gas in the cell is analogous to the photoionized plasmas in the x-ray binary system.

1.5. Describe Z-pinch and Z-machine

The Z-pinch plasma that emits the x-rays which photoionize the gas in our cell is created in the Z pulsed power accelerator at Sandia National Laboratories in Albuquerque, New Mexico. The Z accelerator is the most powerful source of x-rays in the world, producing an x-ray power in excess of 200 TW for an order 100 ns pulse which amounts to a total of 1.9 MJ for the entire pulse (7). It is also the most efficient x-ray source on Earth, converting greater than 10 percent of its input energy into output radiant x-ray energy (4). See Fig. 6 for a photograph of the Z Accelerator at Sandia National Laboratories.

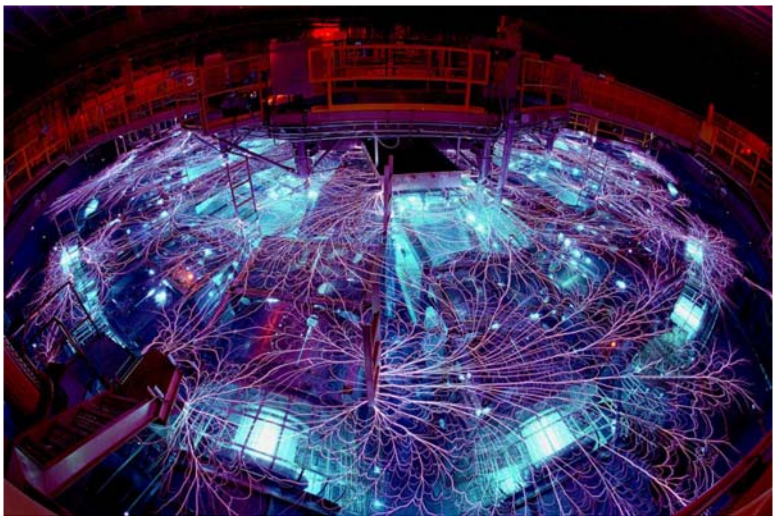

Fig. 6.— The Z Accelerator at Sandia National Laboratories. Shown is an extended exposure photograph of the banking of the pulse-forming switches before a shot. The accelerator tank is filled with de-ionized water which acts an insulator for the capacitors lining the edge of the tank. Unfortunately, the de-ionized water is not a perfect insulator, so that some of the electrical energy stored in the pulse forming switches and transmission lines is able to leak out into the accelerator tank and produce the flashes of electricity along the surface of the water known as flashover arcs which are not unlike strokes of lighting.

As a pulsed-power system, the purpose of the Z accelerator is to convert electrical energy at low powers and long timescales to high powers and short timescales, and then deliver that transformed energy to the Z-pinch load. The Z accelerator accomplishes this using a high-voltage Marx generator to charge an intermediate storage capacitor, which forms the pulse to be delivered to the pinch load. The Marx generator is made up of a number of capacitors lining the rim of the accelerator that are slowly charged in parallel. By utilitizing multiple capacitors, this system increases the voltage delivered to the pinch without requiring an increase in storage capacity of any individual capacitor. Once fully charged, the Marx generator slowly (μs timescales) discharges in series to a cylindrical pulse-forming line (PFL) which acts as an intermediate storage capacitor. Once charged to capacity, the pulse forming line is rapidly (ns timescales) discharged into the Z-pinch load.

A cylindrical array of several hundred tungsten wires acts as the Z-pinch load in these experiments. Historically, single wires were the first loads used in pulsed-power systems, but it was found that one could more efficiently create a high density and temperature plasma by converting the kinetic energy of an imploding material after it has stagnated on the z-axis. In both cases, a large voltage is applied across the load, inducing a large current in the load. The large current vaporizes the wire (or wires, in the cylindrical array case) and creates a low-resistance plasma capable of carrying a large current. Moving charge induces a magnetic field, which means that a current moving in the negative z direction creates a magnetic field directed in the clockwise direction about the pinch. Using the right-hand rule, we see that for a negative z directed current and a clockwise directed magnetic field, the force on any particle is directed inward toward the central axis of the pinch (see Fig. 7). While it is easy to imagine why this is the case for the single wire, it is not so clear why this compression feature would also be characteristic of the wire array. Namely, the individual force vectors due to each differential piece of pinch plasma (except for the piece direcly across from the material in question) either will not point toward the z-axis or they will not be perpendicular to the z-axis. However, all components of the individual force vectors other than those directed toward and perpendicular to the z-axis will cancel with each other due to the symmetry of the system about the z-axis. Thus, for both the single wire and the wire array, the pinch plasma compresses or *pinches* toward the z-axis (hence the names Z-pinch and Z accelerator).

The magnitude of the force on the plasma is quite signficant since the current is of order 10^6 A, so the pinch plasma in the wire array case can be accelerated to a high implosion velocity, of order 10^8 cm s^{-1}. This high implosion velocity is precisely why the wire array system is more effective than the single wire system in creating a high density and high temperature plasma. In order to increase the density and temperature of the plasma produced from the single wire Z-pinch, one can only increase the voltage and power of the pulsed-power system. Using the wire array, however, we are able to increase the strength of the induced magnetic field and thus the implosion velocity and kinetic energy without modifying any parameters of the pulsed-power system. For higher degrees of kinetic energy, more energy is available for conversion when the pinch plasma stagnates on the z-axis, so these plasmas will radiate more x-rays than those with lower kinetic energies.

The Z accelerator is a fast pulsed-power system, delivering its 20 MA current to the load in a short pulse, on the order of 100 ns. This system takes advantage of the feature of pinch plasmas that the plasma will remain stable as long as it has not achieved an equilibrium

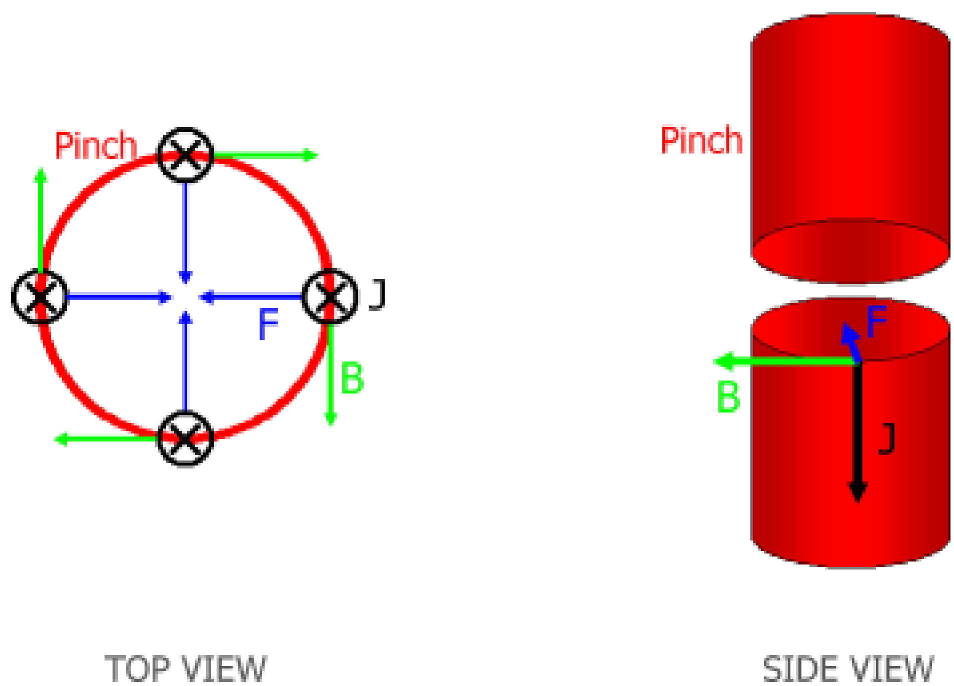

Fig. 7.— Schematic drawings of the $\vec{J} \times \vec{B}$ force on pinch plasma particles. Notice that the force vector points radially inward at each point on in the pinch.

with the magnetic field. Thus, if one can deliver the electrical energy to the load in a shorter pulse, the pinch plasma will implode faster and the growth of magneto Rayleigh-Taylor instabilities leading up to stagnation on the z axis will be minimized. This is precisely what the Z accelerator does, and explains why this facility is one of the most effective in creating highly radiative Z-pinch plasmas.

1.6. Ionization Parameter

For an optically thin environment surrounding a compact x-ray source which is emitting isotropically and homogeneously, we can approximate the radiation field present at radius r as the central source spectrum scaled by geometric dilution. Thus, the flux f received at a location some distance r away from the radiation source is given by the inverse square law,

$$f = L/4\pi r^2 \propto L/r^2, \tag{1.2}$$

where (in cgs units) L is the luminosity in ergs s^{-1}, r is the distance from the source in cm and f is the flux in units of ergs s^{-1} cm^{-2} sr^{-1}.

The state of the gas is described by its (electron) temperature and by the ion populations. If we fix the temperature of the x-ray source (and, thus, its luminosity if we approximate the source as a blackbody) and choose a value for the electron temperature of the gas, then the ionization equilibrium ratios for different charge states depend only on the ionization parameter, which is defined as

$$\xi(r) \equiv L/nr^2 = 4\pi f/n, \tag{1.3}$$

where n is the particle density.

To see why this is the case, I have outlined below a derivation of the ionization parameter given by Duane A. Liedahl in his lecture on the x-ray spectral properties of photoionized plasmas and transient plasmas at the Astrophysics School X (1). We begin by writing an equation of ionization equilibrium, with the ionization processes on one side and the recombination processes on the other. Given a photoionization rate β_i (s^{-1}), a collisional ionization rate C_i (cm^3 s^{-1}), and the recombination rate α_{i+1} (cm^3 s^{-1}) which includes both dielectronic and radiative recombination, the ionization equilibrium equation is of the form

$$n_e C_i n_i + \beta_i n_i = n_e \alpha_{i+1} n_{i+1}, \tag{1.4}$$

where n_e is the electron density, n_i is the density of ions with charge state i, and n_{i+1} is the density of ions with charge state $i+1$. We choose to subsitute for the photoionization rate β which depends on the radiation energy density. At a radius r from the radiation source and for a photon energy of ϵ the energy density $U_\epsilon(\epsilon)$ (erg cm^{-3}) is given by

$$U_\epsilon(\epsilon) = \frac{f_\epsilon(\epsilon)}{c} = \frac{L_\epsilon(\epsilon)}{4\pi r^2 c}, \tag{1.5}$$

where $L_\epsilon(\epsilon)$ is the energy specific luminosity and c is the speed of light. Since the power of the x-ray source for any given photon energy interval is simply a fraction of the total power of the source, we can specify an energy-dependent spectral function which when multiplied to the total luminosity gives the luminosity for a specific energy. Obviously, we should require this spectral function be normalized, such that the fractions for all energies sum together to 1: $\int_{-\infty}^{\infty} f_\epsilon(\epsilon)\,d\epsilon = 1$. Using this normalized spectral function, the energy specific luminosity is given by $L_\epsilon(\epsilon) = Lf_\epsilon(\epsilon)$ (both have units of erg s^{-1} since $f_\epsilon(\epsilon)$ is unitless), so we can rewrite (1.5) as

$$U_\epsilon(\epsilon) = \frac{Lf_\epsilon(\epsilon)}{4\pi r^2 c}. \tag{1.6}$$

If we refer to the energy dependent photoionization cross section of charge state i as $\sigma_i(\epsilon)$ (cm^2) and the photoionization threshold energy (i.e. the minimum photon energy required to ionize an electron of an ion in charge state i) as χ_i, then the photoionization rate β_i will be given by

$$\beta_i = \int_{\chi_i}^{\infty} \frac{c}{\epsilon} U_\epsilon(\epsilon) \sigma_i(\epsilon)\, d\epsilon, \tag{1.7}$$

where we are integrating the photoionization rate over all photon energies greater than the threshold energy of photoionization from start state i to charge state $i+1$. We can simplify this expression as

$$\beta_i = \frac{L}{r^2} \Phi_i, \tag{1.8}$$

where $\Phi_i = \frac{1}{4\pi} \int_{\chi_i}^{\infty} \frac{\sigma_i(\epsilon)}{\epsilon} f_\epsilon(\epsilon)\, d\epsilon$. If we plug this expression for the photoionization rate into (1.4) and then divide by the electron density, we are left with

$$\left(C_i + \xi \Phi_i\right) n_i = \alpha_{i+1} n_{i+1}, \tag{1.9}$$

where we have set the ionization parameter to be

$$\xi = \frac{L}{n_e r^2}, \tag{1.10}$$

as defined in (1.3). Now, we can rearrange (1.9) to

$$\frac{n_{i+1}}{n_i} = \frac{C_i}{\alpha_{i+1}} \left(1 + \frac{\xi \Phi_i}{C_i}\right), \tag{1.11}$$

where $\frac{C_i}{\alpha_{i+1}}$ is equivalent to the collisional ionization equilibrium ratio $\left(\frac{n_{i+1}}{n_i}\right)_{CIE}$. Thus, the term $\frac{\xi \Phi_i}{C_i}$ is a measure of the degree of overionization. Now, as mentioned earlier, if we fix the temperature of the ionizing source (and thus Φ_i) and choose an electron temperature (thereby choosing a value for C_i and α_i), the degree of relative importance of photoionization processes and collisional processes is fully determined by the ionization parameter.

For the gas cell experiment, we can use (1.3) to calculate the ionization parameter at the center of the gas cell at a specific time in the experiment (or simulation). At $t = 100$ ns, the luminosity or power of the pinch is 1.682×10^{21} erg sec^{-1} and the radius is 0.055 cm. Also at that time, at a position near the center of the gas cell, $r_{cell} = 0.578$ cm, the mass density is 3.6×10^{-5} g cm^{-3}. Since the cell is filled with neon gas, we can compute the particle density by dividing the mass density by the the atomic weight of neon and multiplying by the mean number of ionized electrons in the medium. The atomic weight of neon is 20.180 atomic mass units or 3.35×10^{-23} grams, which implies that the ion density is 1.075×10^{18} cm^{-3}. If we approximate the average number of free electrons for every neon ion to be 8.5, then the particle density is approximately 9.138×10^{18} cm^{-3}. We also must compute the radial distance from the pinch to the piece of the gas cell in question, which is simply the sum of the radial distance from the pinch to the face of the gas cell and the gas cell radius. This sum amounts to 6.228 cm, which when combined with the pinch luminosity and particle density, yields an ionization parameter of ~ 5 erg cm s^{-1}. From Fig. 8 we can see that for a cosmic x-ray photoionized nebula the ionization parameter is of order several hundred. Note that in the figure the contours are of $\log(\xi)$, not ξ.

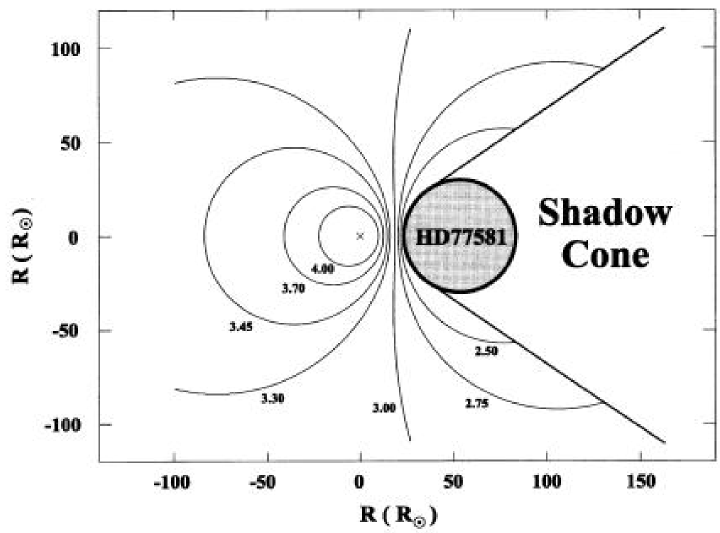

Fig. 8.— Contours of constant ionization parameter (logarithmic) plotted for the region surrounding the HMXRB Vela X-1. (5)

1.7. What is the scope of the thesis?

The scope of my thesis is three-fold. First, simulation codes are used to model a gas-cell experiment (shot Z543) that has already been conducted on the Z machine at Sandia National Laboratories. The absorption spectrum synthesized using the simulation codes is compared to the absorption spectrum measured in the actual experiment. By identifying differences between the synthesized and measured spectra, we are able to calibrate our modeling codes so that they more accurately model the experiment.

Once the codes have been calibrated using experimental data, we are able to enter the second stage of the research: use the same modeling procedure to design new gas cell experiments. Essentially, this equates to testing the effect of changing different experimental parameters, such as gas cell fills, geometries, and positions. If modifying one of these experimental parameters yields an interesting result in the spectrum, then modifying that parameter in the actual experiment may prove to be useful and insightful.

The third and last stage of the research involves using the modeling procedure to synthesize new diagnostics of the photoionized plasma; namely, time dependent absorption and emission spectra. Our goal is to eventually measure these time dependent spectra in the experiment, so it will be important to have synthesized spectra to which we can compare when we conduct the actual observations.

REFERENCES

Netherlands) Astrophysics School (10th: 1997: Amsterdam. *X-ray Spectroscopy in Astrophysics*. Springer, 1999.

D. H. Cohen, J. J. Macfarlane, J. E. Bailey, and D. A. Liedahl. X-ray spectral diagnostics of neon photoionization experiments on the Z-machine. *Review of Scientific Instruments*, 74:1962–1965, March 2003.

D. A. Liedahl, S. M. Kahn, A. L. Osterheld, and W. H. Goldstein. X-ray spectral signatures of photoionized plasmas. *ApJ*, 350:L37–L40, February 1990.

N. R. Pereira and J. Davis. X rays from z-pinches on relativistic electron-beam generators. *Journal of Applied Physics*, 64:1–8979, August 1988.

M. Sako, D. A. Liedahl, S. M. Kahn, and F. Paerels. The X-Ray Spectrum and Global Structure of the Stellar Wind in VELA X-1. *ApJ*, 525:921–934, November 1999.

N. S. Schulz, C. R. Canizares, J. C. Lee, and M. Sako. The Ionized Stellar Wind in Vela X-1 during Eclipse. *ApJ*, 564:L21–L25, January 2002.

R. B. Spielman, C. Deeney, G. A. Chandler, M. R. Douglas, D. L. Fehl, M. K. Matzen, D. H. McDaniel, T. J. Nash, J. L. Porter, T. W. L. Sanford, J. F. Seamen, W. A. Stygar, K. W. Struve, S. P. Breeze, J. S. McGurn, and et al. Tungsten wire-array Z-pinch experiments at 200 TW and 2 MJ. *Physics of Plasmas*, 5:2105–2111, May 1998.

This preprint was prepared with the AAS LaTeX macros v5.0.